

# Reynolds number and surface roughness effects on damping derivatives of the EXOMARS capsule

*Ali Gülhan\* and Josef Klevanski\**

*\*German Aerospace Center (DLR), 51147 Cologne, Germany*

*Marc Dormieux\*\* and Philippe Tran\*\**

*\*\*Astrium Space Transportation, Les Mureaux, France*

*James Merrifield\*\*\**

*\*\*\*Fluid Gravity Engineering Ltd., Emsworth, United Kingdom*

*Stefano Portigliotti\*\*\*\* and Paolo Venditto\*\*\*\**

*\*\*\*\*Thales Alenia Space, Torino, Italy*

*Louis Walpot\*\*\*\*\* and Olivier Bayle\*\*\*\*\**

*\*\*\*\*\*European Space Agency (ESA), Noordwijk, The Netherlands*

## Abstract

Damping derivatives of the Exomars capsule have been measured using free oscillation technique in the Trisonic Windtunnel TMK. A cross flexure instrumented with strain gauges measured the dynamic motion of the model in a Mach number range from 1.8 to 3.5. Reynolds number and angle of attack of the capsule were also varied during experiments. The results show a strong dependency of damping derivatives on the Mach number and angle of attack. Compared to the laminar flow on the smooth surface roughness induced transition seems to effect the dynamic stability of the vehicle remarkably.

## 1. Introduction

Dynamic stability has been one of the major critical issues of entry flights with capsule configurations. Several studies showed the shortcomings of the CFD simulation but also discrepancies between different measurement techniques [1], [4], [5], [6] and [7]. The aerodynamic behavior of the EXOMARS capsule during its entry into the Martian atmosphere is a very important parameter for the success of the mission. In particular the dynamic stability of such configurations in transonic and supersonic flight regimes is critical. The prediction of the dynamic stability using both experimental and CFD tools is quite challenging and requires reliable experimental data on both static and dynamic stability behavior of the vehicle. Therefore in addition to the existing static stability data base of the Exomars EDM configuration dynamic stability tests have been carried out in the DLR Trisonic Windtunnel Cologne in the Mach number range of 1.8 to 3.5.

## 2. Experimental tools

The windtunnel model has a diameter of 100 mm. The front and rear part of the model is made out of an Aluminium alloy and copper, respectively (Figure 1). Additional modular tungsten parts are used to move the center of gravity of the model. The model allows also changing moment of inertia by replacing some tungsten parts with other elements. In order to simulate the real flight configuration the spring cavities on the rear surface of the vehicle were also considered. For correct measurements it is very important to minimize the deviation between the center of gravity (CoG) and the center of rotation (CoR).

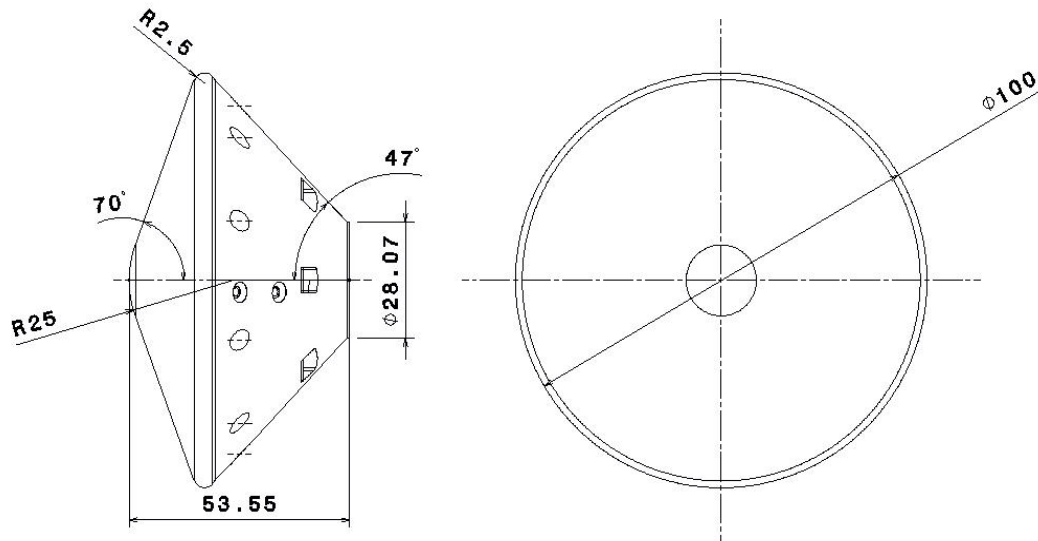


Figure 1: EXOMARS model for dynamic stability measurements

A sketch of the model configuration with integrated instrumentation for the free oscillation tests is shown in Figure 2.

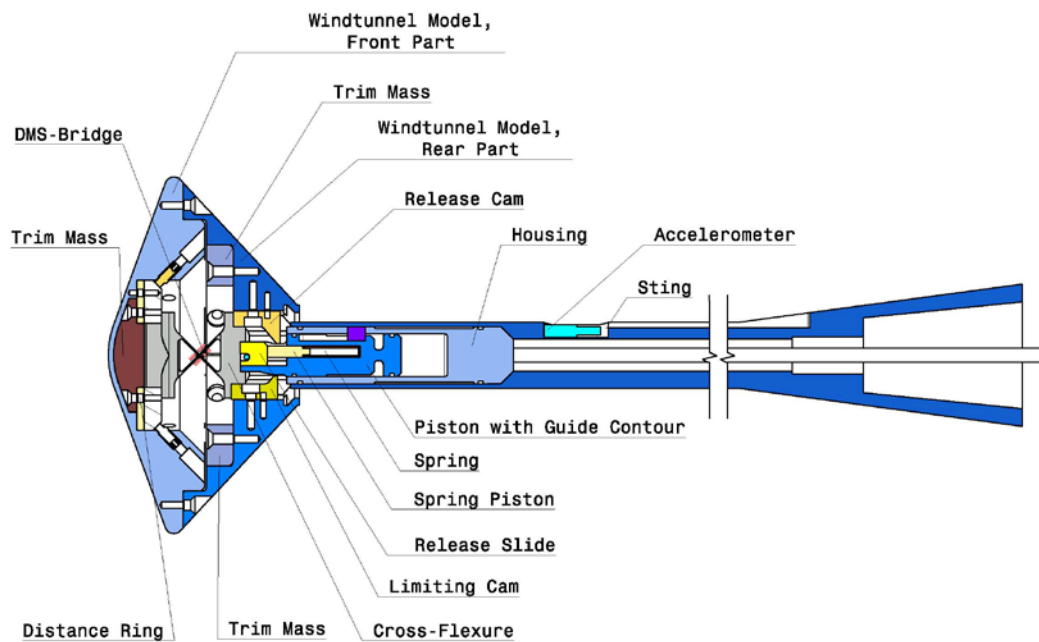


Figure 2: Model configuration of TMK dynamic stability tests

The stiffness of the cross-flexure was defined by considering the duplication requirement with respect to the reduced frequency in addition to Mach and Reynolds numbers duplication. The cross flexure should also allow to get about 20 oscillation cycles for 5 different releases during one run. The cross flexure is made out of a special steel alloy. The EXOMARS model with the integrated cross-flexure is mounted to the sting, which contains the pneumatic release mechanism. The initial amplitude of the oscillation is defined by a release cam. The same system allows also catching the model and stopping the oscillation. The control of the model releasing and catching is provided by a special software in LabView-version.

The cross-flexure is equipped with special strain gauges. The strain gauges were connected to a Wheatstone bridge. The measured DMS-voltage signal corresponds to the deflection angle  $\theta$  of the cross-flexure. The sting is made out of a steel alloy. It is designed to minimize the interaction with wake: The sting length - model diameter ratio is above

3.55 ( $L_{\text{sting}}/D_{\text{ref}} > 3.55$ ) and sting diameter - model diameter ratio is less than 0.18 ( $D_{\text{sting}} / D_{\text{ref}} < 0.18$ ). The model configuration for dynamic stability measurement in TMK is shown in Figure 3.

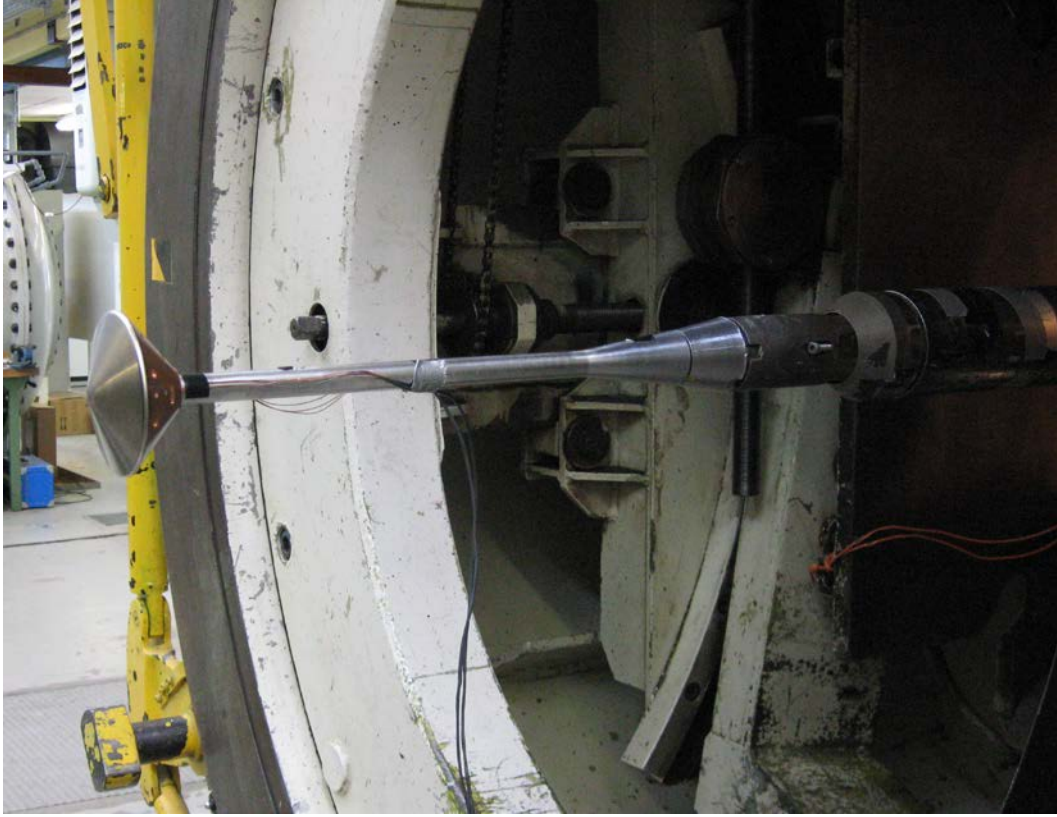


Figure 3: EXOMARS model for dynamic stability measurements in TMK

### 3. Calibration of the cross flexure

#### 3.1 Static calibration

The cross-flexure stiffness and the calibration factor of the DMS for the measurement of deflection angle is determined by the static calibration performed with the special static calibration device, which is fixed to the special movable support (see Figure 4).

The mechanical moment is produced by placing of the etalon masses on the several pre-defined positions of the horizontal bar of the calibration device (Figure 4). The resulted deflection of the calibration device due to the cross-flexure deformation is compensated by the rotation of the support sting. The horizontal orientation of the horizontal bar was restored and the compensating angle of the support equals exactly to the cross-flexure deformation. The compensation angle of the support is measured with both electronic sensors and by the spirit level. The electrical output signal of the DMS is also measured.



Figure 4: Static Calibration Device

After compensation of the Zero-deviation the linear regressions for DMS calibration were performed. The mechanical stiffness (as a linear regression) for the cross-flexure is shown in Figure 5. Static calibration leads to a cross flexure stiffness of  $C_y = -4.1 \text{ Nm/rad}$ .

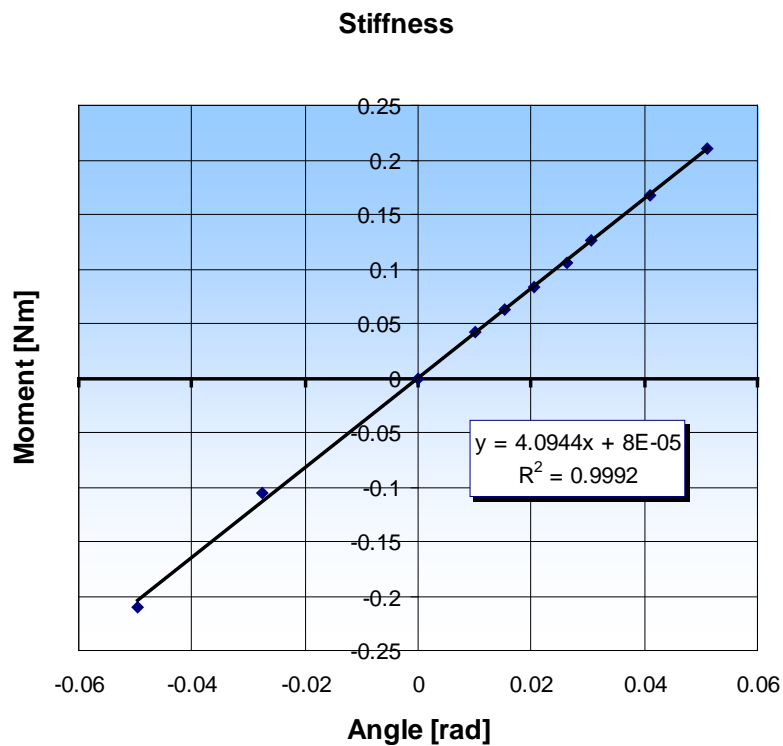


Figure 5: Static calibration curve

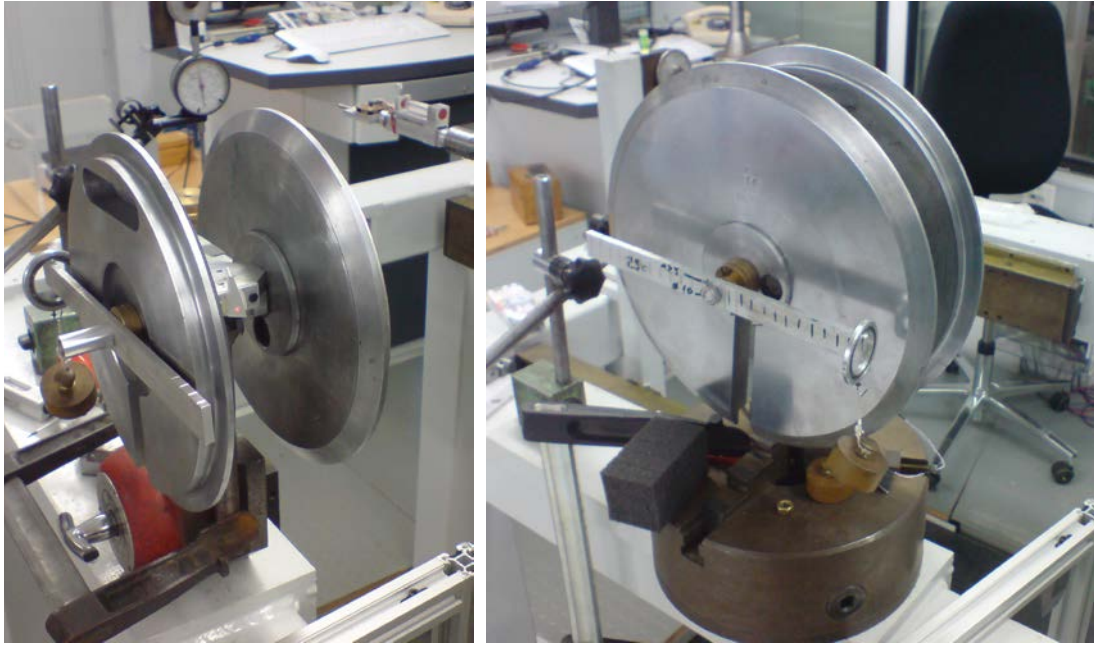


Figure 6: Static Calibration Device: Axial force by balanced disk weights

The increase of the flexure stiffness as a result of the axial stress was experimentally studied and the trend dependency  $C_y = f(F_x)$  was determined. This phenomenon was also verified by a finite element analysis (FEM). A special static calibration device was developed for determination of the increase of the flexure stiffness  $C_y = f(F_x)$  due to the acting axial force. It uses balanced disk weights (Figure 6). The estimated stiffness data are given in the diagram below: Stiffness Data estimated via Calibration Device (v.2) are given in Figure 7.

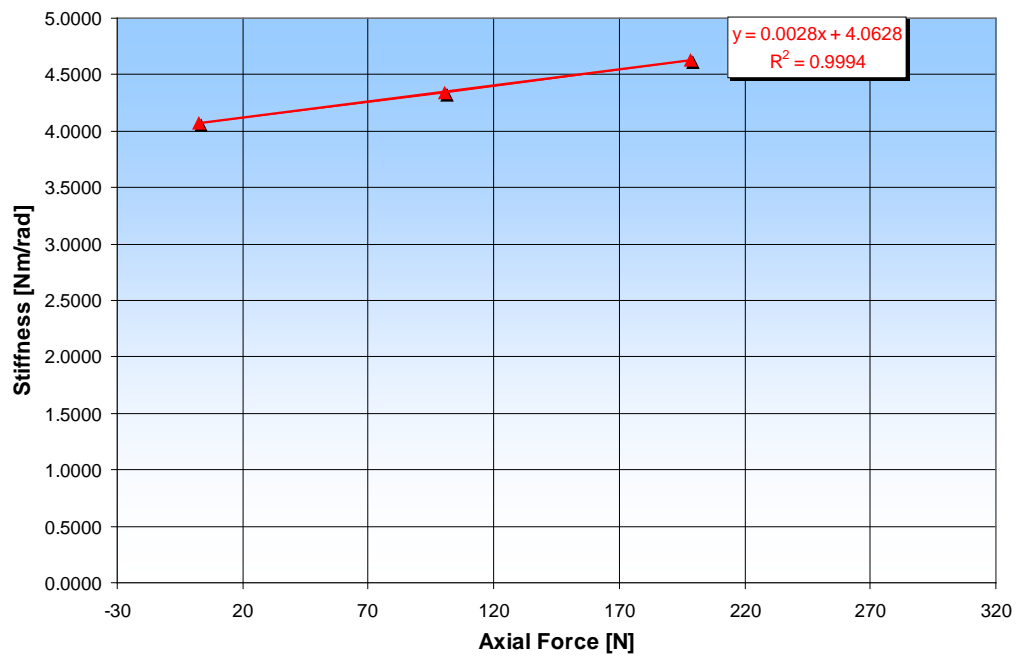


Figure 7: Static calibration stiffness dependency on the axial force:  $C_y = f(F_x)$

### 3.2 Dynamic calibration

The main objectives of the dynamic calibration are to estimate the moment of inertia of the wind tunnel model  $I_y$  and the damping characteristic of the flexure without flow  $k_y(\omega)$ . For this task a specially designed dynamic calibration device was used (see Figure 8). It has special catches for the etalon disks, with the known geometry and inertia characteristics. This device is fixed to the cross-flexure and both are mounted to the sting which contains the release mechanism. The free oscillations are initiated via this release mechanism.

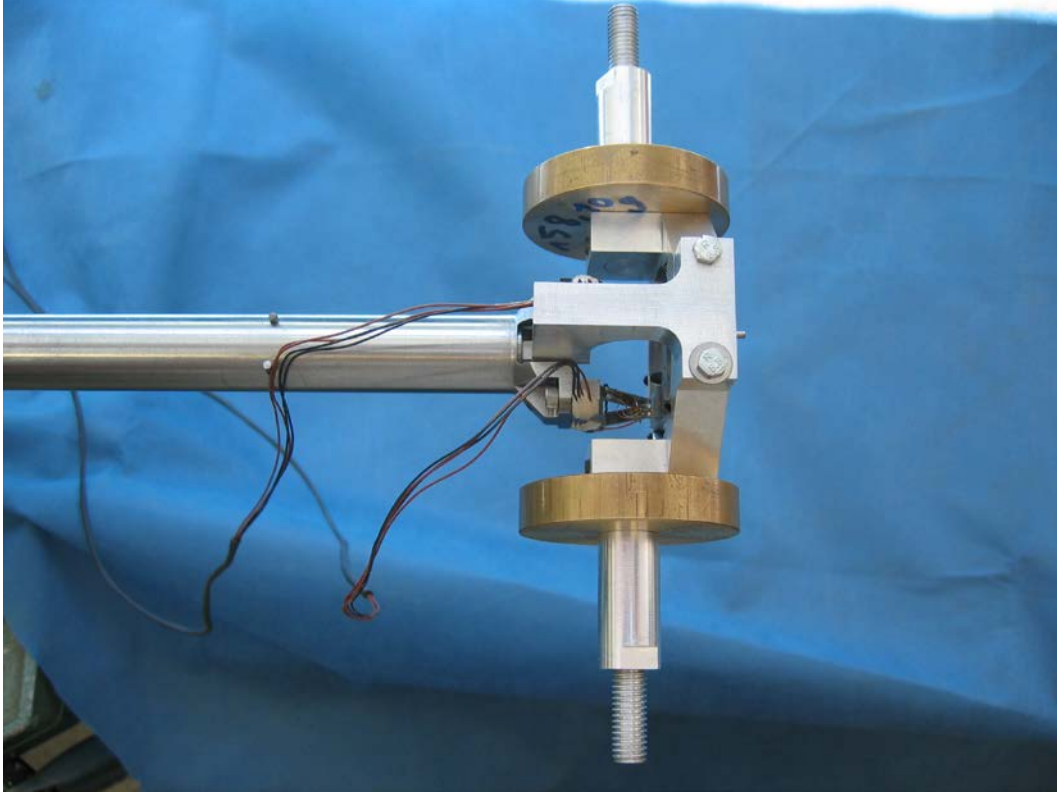


Figure 8: Dynamic Calibration Device

The moment of inertia was estimated from the dynamic calibration curves shown in Figure 9. The linear regression was used to describe the dependency of the moment of inertia on the frequency, i.e.  $I_{y \text{ Disc Comb}} = f(1/\omega^2)$  (see deep blue line in Figure 9). The regression coefficients 4.449 correlates very well with the value coming from the static calibration of the cross-flexure ( $c_y=4.46$ ). The regression shift corresponds very well to the moment of inertia of the dynamic calibration device:

$$I_{y \text{ Device}} = 6.59299\text{E-}05 \text{ kg}\cdot\text{m}^2$$

The moment of inertia of the model can be easily calculated as  $I_y = c_y / \omega^2 = 0.00045 \text{ kg}\cdot\text{m}^2$

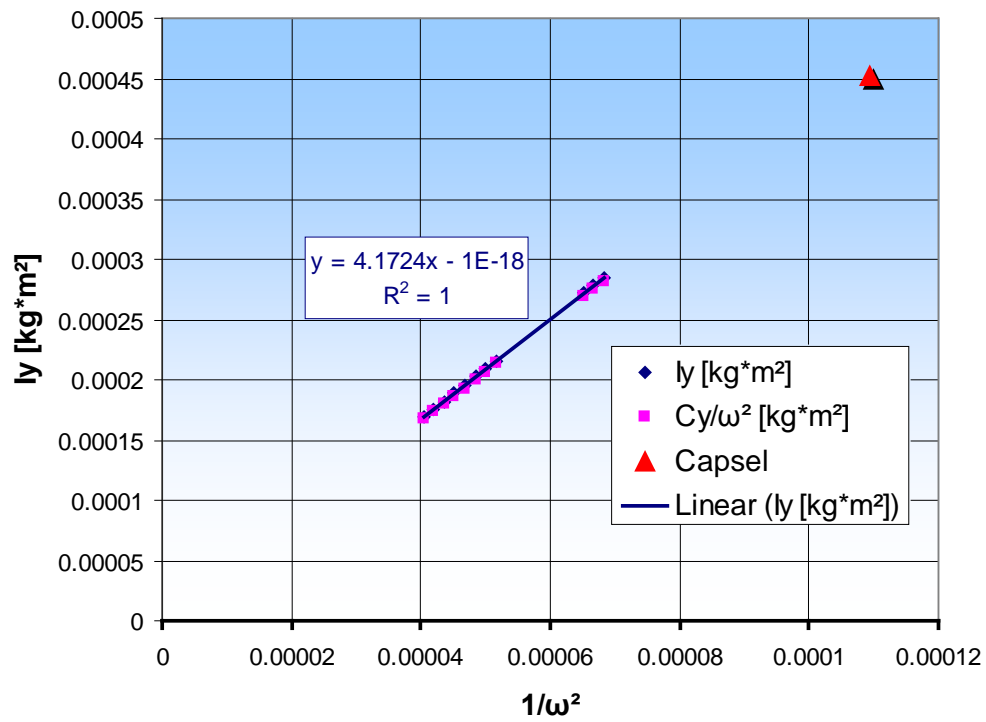


Figure 9: Estimation of the Model Inertia

To check the influence of the atmosphere conditions on the damping the dynamic calibration was carried in the vacuum chamber of the wind tunnel H2K. During the dynamic calibration campaign the special features of the cross-flexure were investigated in details. Very good reproducibility of the data has been noticed for different releases for both cross-flexures. No amplitude dependency of the damping has been noticed for the cross-flexure. The cross-flexure damping depends on the oscillation frequency (see Figure 10). Therefore the disc combinations are specially defined to cover the necessary frequency range.

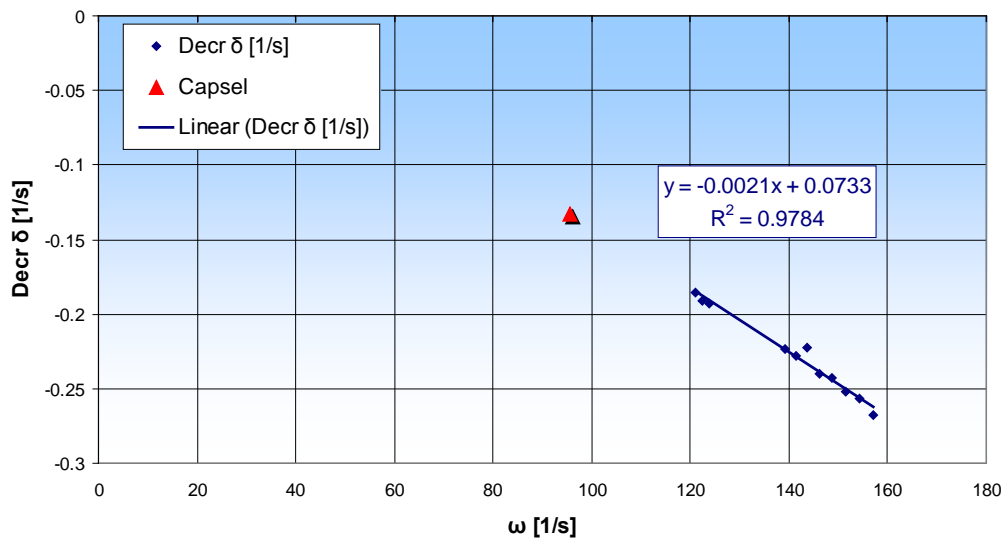


Figure 10: Damping Characteristic of the flexure

The identification method applied for the damping decrement  $\delta$  and the estimation of the oscillation frequency  $\omega$  based on the free oscillation tests data processing are described in the section 4.

## 4. Damped oscillation

In TMK the dynamic derivatives of the EXOMARS capsule are estimated via free oscillation method, which analyses free oscillation of the scaled capsule model fixed on a sting by means of a cross flexure with and without supersonic flow. It is to note that in this case it is only possible to estimate the sum of the dynamic derivatives  $c_{m\dot{\alpha}} + c_{mq}$  because it is impossible to separate the angle of attack change from the pitch rate due to the kinematical motion limitations by oscillation round the rotation center.

### 4.1 Basic relations

If we consider the motion of the capsule model fixed on the cross-flexure placed in the flow as the model deflections relative to the trimmed position (under assumption that these deflection are small) we can formulate the differential equation for the free oscillation as:

$$I_y \ddot{\theta} + (k_y + M_{\dot{\theta}}) \dot{\theta} + (c_y + M_{\theta}) \Delta \theta = 0 \quad (1)$$

where  $I_y$  is moment of inertia,  $k_y$  is mechanical damping coefficient,  $c_y$  represents mechanical stiffness coefficient,  $M_{\dot{\theta}}$  is aerodynamic damping and  $M_{\theta}$  is aerodynamic stiffness,  $\Delta \theta$  represents here the deflection angle. In case of the flow parallel to the sting axis deflection angle equals to the angle of attack:

$$\phi = 0; \quad \theta = \alpha.$$

The first term  $I_y \ddot{\theta}$  represents the inertia; the second term  $(k_y + M_{\dot{\theta}}) \dot{\theta}$  represents damping and the third term  $(c_y + M_{\theta}) \theta$  the elasticity.

If the capsule model is placed in vacuum (no flow influence, aerodynamic damping  $M_{\dot{\theta}} = 0$  and aerodynamic stiffness  $M_{\theta} = 0$ ) then the equation 1 can be written as:

$$I_y \ddot{\theta} + k_y \dot{\theta} + c_y \theta = 0 \quad (2)$$

The ansatz for the analytic solution for the damped harmonic oscillation (basic solution of the equation 1) is:

$$\theta = \hat{\theta} e^{-\delta t} e^{i\omega t} \quad (3)$$

Here  $\hat{\theta}$  represents the oscillation amplitude and  $\delta$  represents the oscillation decrement.

The first derivative of  $\theta(t)$  is:

$$\dot{\theta} = \hat{\theta} e^{-\delta t} e^{i\omega t} (-\delta + i\omega) \quad (4)$$

and the second derivative of  $\theta(t)$  yields:

$$\ddot{\theta} = \hat{\theta} e^{-\delta t} e^{i\omega t} (\delta^2 - 2i\delta\omega - \omega^2) \quad (5)$$

Substituting equations 3, 4 and 5 into equation 1 and separation of the real and imaginary part of solution yields:

$$\text{Re: } I_y (\delta^2 - \omega^2) - (k_y + M_{\dot{\theta}}) \delta + (c_y + M_{\theta}) = 0 \quad (6)$$

$$\text{Im: } -I_y 2\delta + (k_y + M_{\dot{\theta}}) = 0 \quad (7)$$

From equations 6 follows:

$$(c_y + M_{\theta}) = -I_y (\omega^2 - \delta^2) \quad \text{with } \delta \ll \omega \quad (8)$$

and

$$\omega_{va} = \sqrt{-\frac{c_y}{I_y}}; \quad \omega_{wt} = \sqrt{-\frac{c_y + M_\theta}{I_y}} \quad (9)$$

From equations 7 yields:

$$(k_y + M_\theta) = 2I_y \delta \quad (10)$$

Assuming the damping decrement  $\delta$  and the oscillation frequency  $\omega$  are determined with and without of flow influence and mechanical damping  $k_y$ , mechanical stiffness  $c_y$  of the cross-flexure and the inertia moment of the capsule model  $I_y$  are known, we can easily calculate both the aerodynamic stiffness and the aerodynamic damping:

$$M_\theta = -I_y \omega_{wt}^2 - c_y = I_y (\omega_{va}^2 - \omega_{wt}^2) \quad (11)$$

$$M_\theta = 2I_y \delta_{va} - k_y \quad (12)$$

Finally the dimensionless derivatives can be calculated using following relations:

$$c_{m\alpha} = M_\theta / \left( \frac{\rho}{2} u_\infty^2 S_{ref} D_{ref} \right) \quad (13)$$

$$(c_{m\dot{\alpha}} + c_{mq}) = 2u_\infty M_\theta \left( \frac{\rho}{2} u_\infty^2 S_{ref} D_{ref}^2 \right) \quad (14)$$

The stiffness  $c_y$  and the mechanical damping  $k_y$  of the cross-flexure and the inertia moment of the capsule model  $I_y$  is estimated via static and dynamic calibration tests.

The increase of the flexure stiffness  $C_y = f(F_x)$  measured during static calibration of the cross-flexure is taken into account. The axial Force  $F_x$  during the wind tunnel tests is calculated as

$$F_x = c_x(Ma, \alpha) \left( \frac{\rho}{2} u_\infty^2 S_{ref} \right) \quad (15)$$

where the axial force coefficient  $c_x(Ma, \alpha)$  is taken from the static tests [2]. Here is to remark that the  $c_x$  dependency of the angle of attack can be neglected for the small angle ( $\alpha < 10^\circ$ ):

$$c_x(Ma, \alpha) \approx c_x(Ma, \alpha = 0^\circ) \quad (16)$$

## 4.2 Calculation of the damping decrement

The damping decrement  $\delta$  and the free oscillation frequency  $\omega$  are calculated on basis of the recorded oscillation data as the nonlinear regression model parameters via special identification routine **R2LIN** from the **IMSL**-library, based on the mean square method [8].

The nonlinear regression model is in general case

$$y_i = f(x_i, \theta) + \varepsilon_i, \quad i = 1, 2, \dots, n \quad (17)$$

where the observed values of the  $y_i$ 's constitute the responses or values of the dependent variable, the  $x_i$ 's are the known vectors of values of the independent (explanatory) variables,  $f$  is a known function of an unknown regression parameter vector  $\theta$ , and the  $\varepsilon_i$ 's are independently distributed normal errors each with mean zero and variance  $\sigma^2$ .

For this model, a least squares estimate of  $\theta$ , is also a maximum likelihood estimate of  $\theta$ . The residuals for the model are:

$$e_i(\theta) = y_i - f(x_i, \theta) = y_i - (\theta_1 e^{\theta_2 t_i} \cos(\theta_3 t_i + \theta_4) + \theta_5) \quad (18)$$

A value of  $\theta$  that minimizes

$$\sum_{i=1}^n [e_i(\theta)]^2 \Rightarrow \min \quad (19)$$

is a least squares estimate of  $\theta$ .

To estimate the values of  $\theta$ , which correspond to the minimum, the equation 19 is to partially differentiate, set to 0 and to solve with respect to  $\theta$ .

$$\frac{\partial e_i(\theta_k)}{\partial \theta_k} = \frac{\partial (y_i - f(x_i, \theta_k))}{\partial \theta_k} = -\frac{\partial f(x_i, \theta_k)}{\partial \theta_k} = 0 \quad (20)$$

Routine **R2LIN** is designed so that these residuals are input one at a time from a user-supplied subroutine. This permits **R2LIN** to handle the case when  $n$  is large and the data cannot reside in an array but must reside on some secondary storage device.

Routine **R2LIN** is based on MINPACK routines LMDIF and LMDER by Moré et al. (1980). The routine **R2LIN** uses a modified Levenberg-Marquardt method to generate a sequence of approximations to a minimum point.

For the damping harmonic oscillation solution ansatz (equation 3) the nonlinear regression can be written in form:

$$y_i = \theta_1 e^{\theta_2 t_i} \cos(\theta_3 t_i + \theta_4) + \theta_5 \quad (21)$$

If we compare nonlinear regression 21 with ansatz 3 we conclude that:

$$\hat{\theta} = \theta_1; \quad \delta = \theta_2; \quad \omega = \theta_3 \quad (22)$$

To improve the iteration convergence of the **R2LIN** the nondefault convergence parameters preliminary established with the special **R8LIN** routine are used.

The correct choose of the initial values of  $\theta_1 \dots \theta_5$  is very important for the iteration convergence of the routine **R2LIN**. To improve the iteration convergence the data pre-processing will performed. The useable regions of data will be chosen. For these regions the mean values will be estimated. Mean is used as the initial value for  $\theta_5$ . Based on the preliminary established local minimum/maximum values the initial values for amplitude  $\theta_1$  and for frequency  $\theta_3$  and will be estimated. The initial value for the phase shift  $\theta_4=0$ , because the start and end points of the regions corresponds to the local minimums/maximums. The damping decrement  $\theta_2$  will be initially set to 0.

Figure 11 shows the original (measured) data in comparison with the data reconstructed by regression 21 and demonstrates the high quality of the reconstruction.

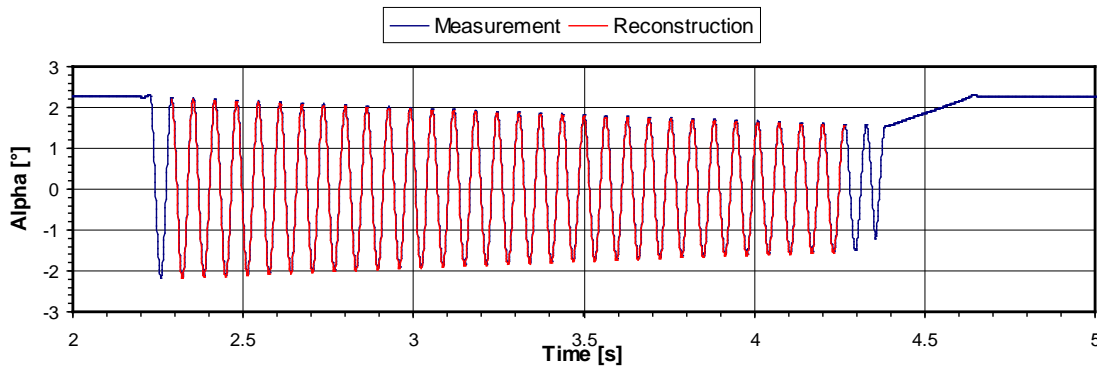


Figure 11: Original Measurement Data(blue) and Reconstructed Data(red)

## 5. Flow parameters

For the duplication of the flight Reynolds number the ejector operation mode of TMK was used. The ejector mass flow rate tuned in such a way that the flight Reynolds number based on the model diameter of 0.1 m was set to approx.  $1.10^6$ . The flow parameters computed from the measured reservoir pressure and total temperature with the known nozzle geometry, i.e. Mach number are listed in Table 1.

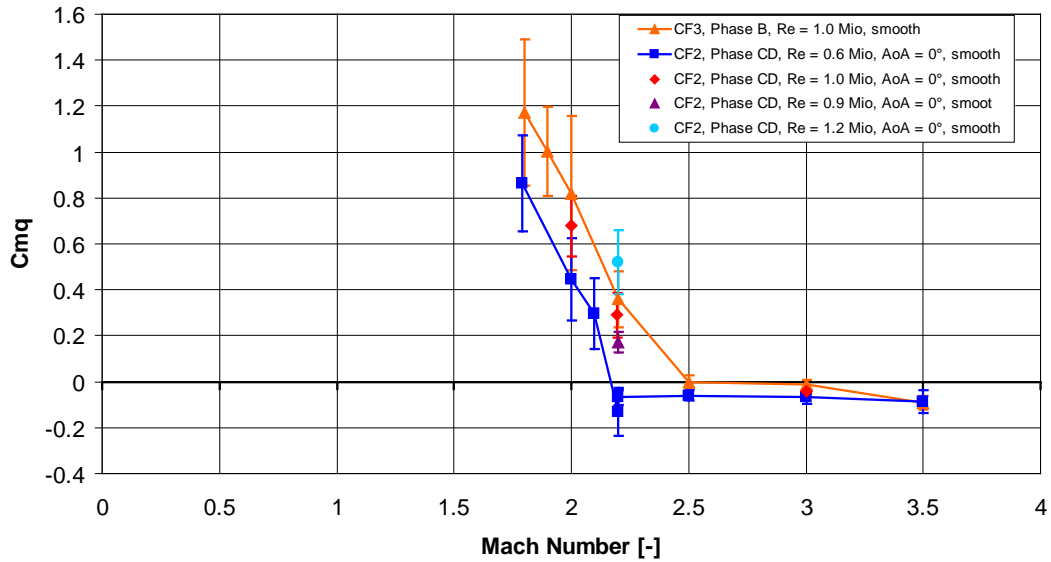
Table 1: Flow parameters of TMK tests

Ma [-]	$p_1$ [bar]	$u_1$ [m/s]	$q$ [bar]
1.8	0.0717	476.6	0.163
2	0.0728	507.2	0.204
2.1	0.0645	519.1	0.199
2.2	0.0527	533.1	0.179
2.5	0.0420	566.8	0.184
3	0.0219	609.9	0.138
3.5	0.0151	641.6	0.129

## 6. Experimental results

### 6.1 Tests at different angles of attack

Tests at  $0^\circ$  angle of attack have been performed at two different Reynolds numbers. Originally the flight Reynolds number in the low supersonic regime was defined as 1 Mio [1]. The first test campaign was carried out at these flow conditions. During the second test campaign, which has been carried out roughly one year later, the Reynolds number of 1 Mio has been decreased to 0.6 Mio due to the changes in the flight trajectory of the Exomars EDM capsule. In order to check the repeatability of the facility parameter and measurement technique the first comparative test has been performed at  $Re = 1$ Mio. As shown in Figure 12 the data is in a very good agreement with the results of the previous test campaign. At  $Re=1$  Mio the capsule has an escalating behaviour at Mach numbers below 2.5. Because of the limitation of the deflection angle to  $4^\circ$  it cannot be determined, whether the capsule reaches a limit cycle. The data at  $Re = 0.6$  Mio show the same trend but the escalating behaviour is shifted to lower Mach numbers below  $Mach=2.2$ .


Figure 12: Pitch damping coefficient derivative at  $0^\circ$  angle of attack

The influence of the Reynolds number by  $Ma = 2.2$  at  $0^\circ$  angle of attack has been clearly demonstrated by varying the Reynolds number between 0.6 Mio and 1.24 Mio as shown in the Figure 13.

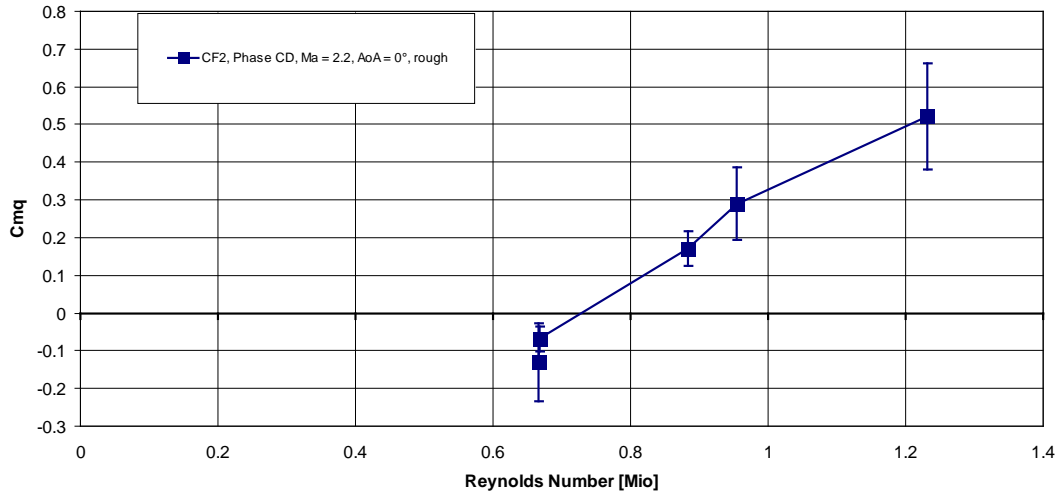


Figure 13: Pitch damping coefficient derivative vs. Reynolds Number at  $Ma = 2.2$

The results of several experiments at different angles of attack are shown in Figure 14. For  $Re=1$  Mio at an angle of attack of  $1^\circ$  the capsule is stable for Mach numbers higher than 2.5, unstable for Mach numbers below 2.5 and indifferent for Mach 2.5. The Mach range with stable capsule behaviour is same as with  $0^\circ$  angle of attack, but the configurations are always more stable, especially at low Mach numbers. There is nearly no difference between  $2.0^\circ$  and  $4.0^\circ$  angle of attack at Mach 1.8. At angle of attack of  $4^\circ$  a damped oscillation was noticed for all tested Mach numbers (1.8 to 3.5). The results show a strong dependency of the pitch damping derivative on the angle of attack.

For  $Re=0.6$  Mio. at an angle of attack of about  $1^\circ$  the capsule is dynamically stable for Mach numbers higher than 2.5, indifferent for Mach 2.2 and has an escalating behaviour for Mach numbers below 2.5. The Mach range with stable capsule behaviour is practically the same as with  $0^\circ$  angle of attack. With the further increasing of the angle of attack to  $1.5^\circ$  and to  $1.7^\circ$  the capsule behaviour becomes less unstable, especially for the Mach numbers bellow 2.2. Here is to mention that some dependency of the oscillation behaviour on the initial deflection has been observed.

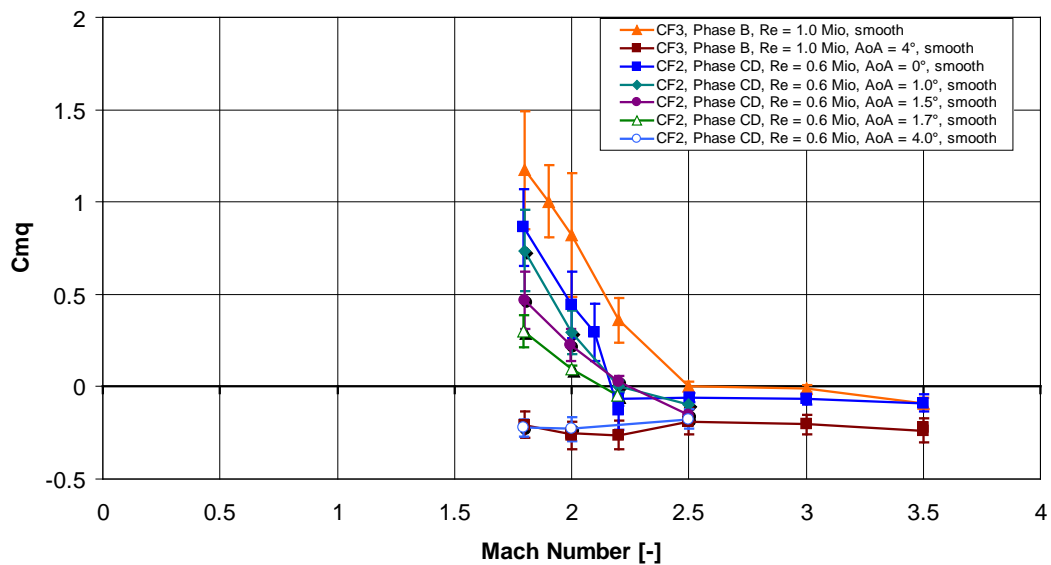


Figure 14: Pitch damping coefficient derivative for different angles of attack

## 6.2 Tests with surface roughness

In order to check the influence of the surface roughness on the on the dynamic stability behaviour, a distributed roughness of 80  $\mu\text{m}$  was applied to the capsule front surface. With rough surface the capsule becomes a little bit more stable (but still unstable) below Mach 2.5. But its escalation behaviour becomes stronger above Mach 2.5. This can be seen in Figure 15.

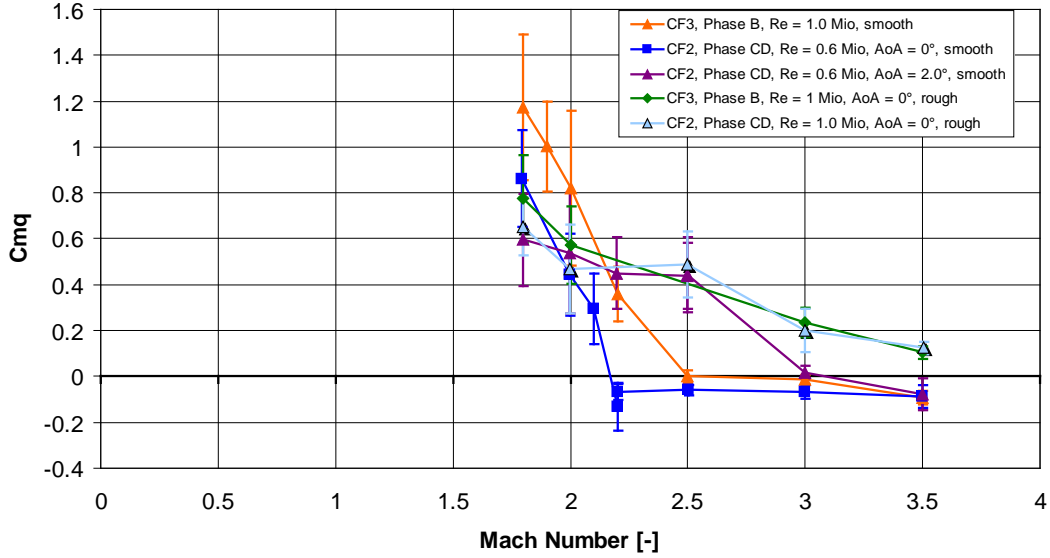


Figure 15: Pitch damping coefficient derivative for different surface roughnesses

## 6.3 Pitch static coefficient derivative

The pitch static coefficient derivative  $c_{m\alpha}$  values are estimated by free oscillation method according to the formula:

$$c_{m\alpha} = \frac{I_y (\omega_{va}^2 - \omega_{wt}^2)}{q_\infty S_{ref} D_{ref}} \quad (21)$$

The  $c_{m\alpha}$  values estimated on basis of the nonlinear static momentum characteristics  $c_m(\alpha)$  given in as

$$c_{m\alpha} = \frac{\partial c_m(\alpha)}{\partial \alpha} \quad (22)$$

The axial Force  $F_x$  during the wind tunnel tests is calculated as:

$$F_x = c_x(Ma, \alpha) \left( \frac{\rho}{2} u_\infty^2 S_{ref} \right) \quad (23)$$

where the axial force coefficient  $c_x(Ma, \alpha)$  is taken from the [2]. Here is to remark that the  $c_x$  dependency of the angle of attack can be neglected for the small angle ( $\alpha < 10^\circ$ ):

$$c_x(Ma, \alpha) \approx c_x(Ma, \alpha = 0^\circ) \approx 1.5 \dots 1.55 \quad (24)$$

The pitch static coefficient  $c_{m\alpha}$  values estimated by the free oscillation method and the  $c_{m\alpha}$  values estimated by static tests are both presented in the Figure 16.

Over both test campaigns most of the tests have been carried out at  $Ma=2$ . Therefore the comparison in Figure 16 shows the data at this Mach number. After a small transition range  $c_{m\alpha}$  becomes almost constant at angles of attack higher than  $\pm 2^\circ$ . At further Mach numbers data only limited data is available and therefore a graphical description of the results is not suitable. But as mentioned in different studies  $c_{m\alpha}$  remains almost constant for supersonic Mach

numbers. The data of the pitch static coefficient  $c_{ma}$  values estimated by the free oscillation method are in a satisfactory good agreement with the  $c_{ma}$  values estimated by static tests.

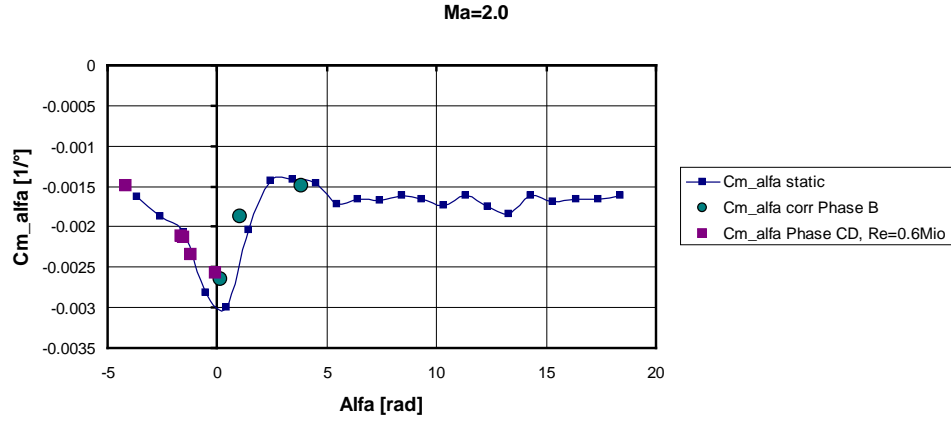


Figure 16: Comparison of static Pitch derivaiva derived from static and dynamic tests at Ma=2.0

#### 6.4 Wake flow analysis

Schlieren pictures of the wake flow were very useful to analyse the wake flow. For all tests a well established flow field has been observed. In addition, in order to compare the wake flow, which dominates the dynamic stability behavior of the capsule, Schlieren pictures of different test configurations have been compared using the wake flow size described with the parameters shown in Figure 17.

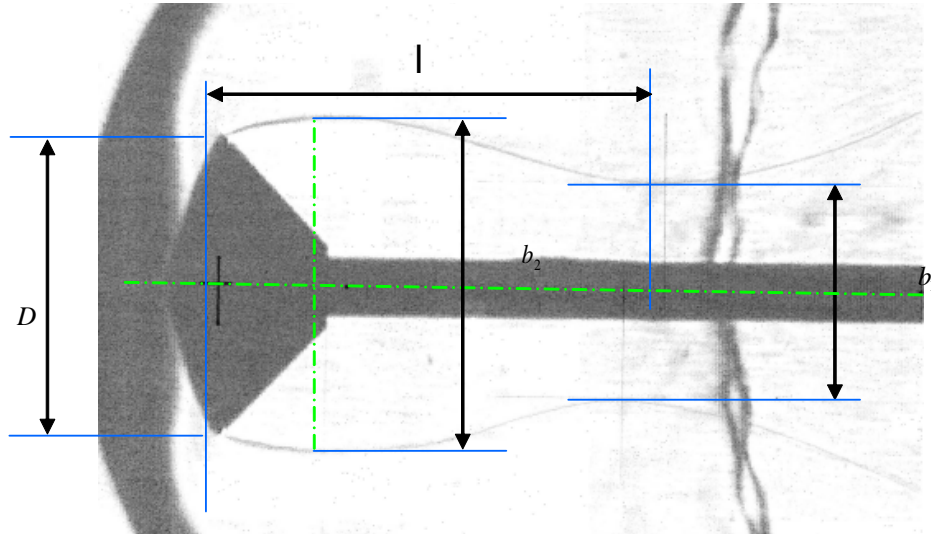


Figure 17: Characteristics of the wake flow

Measured wake flow geometry parameters with corresponding pitch derivative coefficient are listed in Table 2.

Table 2: Wake size depending on the Mach number and surface property

surface	Ma	2.0	3.0	3.5
smooth	$b_2/D$	1.09	0.95	0.93
	$l/D$	n.m.	1.19	1.21
	$c_{mq}$	0.821	-0.012	-0.092
rough	$b_2/D$	1.11	0.98	0.95
	$l/D$	n.m.	1.16	1.18
	$c_{mq}$	0.574	0.236	0.104

The parameter  $b_1/D$  was difficult to measure accurately and therefore is not included in the table. The data of tests on smooth surface shows that the wake diameter decreases by increasing the Mach number. Since a clearly measurable dependency of the wake diameter ( $b_2/D$ ) and pitch derivative ( $c_{mq}$ ) on the Mach number has been noticed, a remarkable change of the flow topology around the capsule edge is expected. Therefore the geometry of the capsule cone edge seems to be an important parameter to influence the dynamic stability of the vehicle.

For the rough surface a similar dependency of  $b_2/D$  and  $c_{mq}$  on the Mach number has been measured. But the sensitivity is weaker. Although  $b_2/D$  gets bigger compared to the smooth surface case, the capsule has stronger escalating behavior at Mach numbers between 2.5 and 3.5.

A Reynolds number increase seems to cause similar effects like the application of surface roughness, since both measures lead to boundary layer transition and turbulent flow on the front surface of the capsule.

## 7. Concluding remarks

The main results of the test campaign with respect to the dynamic stability of the EXOMARS capsule can be summarized as follows:

- At flight Reynolds number  $Re = 0.6$  Mio and at  $0^\circ$  angle of attack the Exomars capsule with a smooth surface is dynamically stable at Mach numbers above 2.2.
- At flight Reynolds number  $Re = 0.6$  Mio and at angle of attack  $1^\circ$ ,  $1.5^\circ$  and  $1.7^\circ$  the Exomars capsule with a smooth surface is dynamically stable at Mach numbers above 2.2.
- At flight Reynolds number  $Re = 0.6$  Mio and at  $4^\circ$  angle of attack the Exomars capsule with a smooth surface is dynamically stable at Mach numbers between 1.8 and 3.5.
- Tripping the boundary layer flow on the front surface changes the dynamic stability behaviour of the capsule significantly.
- At flight Reynolds number and angle of attack of  $0^\circ$  the Exomars capsule with a rough surface, i.e. tripped boundary layer flow, becomes dynamically more stable at low Mach numbers (below 2.2) and tends to have an escalating behaviour at Mach numbers between 2.5 and 3.5. Because of limitation of the deflection angle to  $4^\circ$  during experiments, it is not possible to predict the limit cycle angle of the capsule.
- Schlieren pictures indicate that during tests with the smooth surface at flight Reynolds number the wake size increases by decreasing the Mach number and results in higher dynamic pitch instability.
- The presence of the sting in the windtunnel test configuration could have an important contribution to the dynamic stability behavior of the capsule and needs to be investigated in more details using complementary experimental und numerical tools.

## 8. Acknowledgements

The authors express their special acknowledgement to the European Space Agency (ESA) for its financial and technical support. This work has been carried out under ESA funding of the Exomars Project. Thales Alenia Space Italia is prime contractor for the EDM development

## References

- [1] Gülhan, A., Klevanski, J., Willems, S.; *Experimental study of the dynamic stability of the EXOMARS capsule*, Proceedings of the 7<sup>th</sup> European Symposium on Aerothermodynamics, 2011
- [2] Gülhan, A., Tarfeld, F., Achner, M.; *Static Stability Tests on the EXOMARS Capsule in the DLR Trisonic Windtunnel TMK* DLR Report DLR-EXOMARS-SS-TMK-TR. 2008
- [3] Klevanski, J., Achner, M., Willems, S., Gülhan, A.; *Dynamic Stability Tests on the EXOMARS Capsule in the DLR Trisonic Windtunnel TMK Phase CD*, DLR Report EXM-DM-TRP-DLR-0003, 2012
- [4] Cheatwood F. McNeil, Winchenbach Gerald L., Hathaway Wayne, Chapman Gary; *Dynamic Stability Testing of the Genesis Sample Return Capsule*, AIAA-2000-1009.
- [5] Schoenberger Mark, Hathaway Wayne, Yates Laslie, Desai Presun; *Ballistic Range Testing of the Mars Exploration Rover Entry Capsule*, AIAA-2005-0055
- [6] Murman Scott M., Aftosmis Michael J.; *Dynamic Analysis of Atmospheric-Entry Probes and Capsules*, AIAA-2007-0074.
- [7] Edquist K. T., Desai P. N., Schoenenberger M.; *Aerodynamics for the Mars Phoenix Entry Capsule*, AIAA 2008-7219.
- [8] IMSL. Fortran Subroutines for Statistical Applications. Stat Library Volume 1.